Circular dichroism second-harmonic generation microscopy probes the polarity distribution of collagen fibrils

Margaux Schmeltz, Claire Teulon, Maxime Pinsard, Uwe Hansen, Maged Alnawaiseh, Djida Ghoubay, Vincent Borderie, Gervaise Mosser, Carole Aimé, François Légaré, et al.

Research Article Vol. 7, No. 11 / November 2020 / Optica 1469

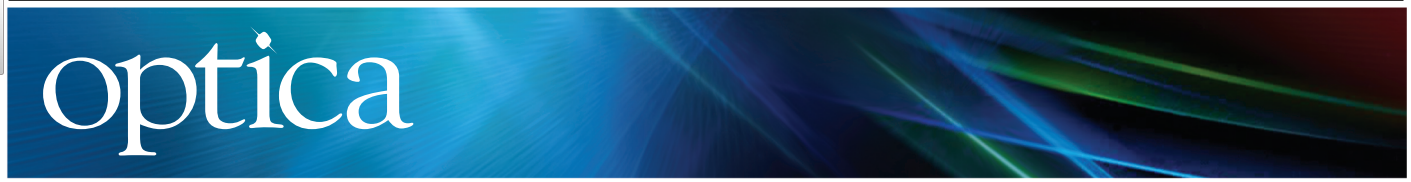

Circular dichroism second-harmonic generation microscopy probes the polarity distribution of collagen fibrils

Margaux Schmeltz,[1] Claire Teulon,[1] Maxime Pinsard,[2] Uwe Hansen,[3] Maged Alnawaiseh,[4] Djida Ghoubay,[5] Vincent Borderie,[5] Gervaise Mosser,[6] Carole Aimé,[6,7] François Légaré,[2] Gaël Latour,[1,8] and Marie-Claire Schanne-Klein[1,*]

[1]Laboratoire d'Optique et Biosciences, École polytechnique, CNRS, Inserm, Institut Polytechnique de Paris, F-91128 Palaiseau, France
[2]Institut National de la Recherche Scientifique, Centre Energie Matériaux et Télécommunications, Varennes, Québec J3X 1S2, Canada
[3]Institute for Musculoskeletal Medicine, University Hospital Münster, 48149 Münster, Germany
[4]Department of Ophthalmology, University of Münster Medical Center, 48149 Münster, Germany
[5]Sorbonne Université, CHNO des Quinze Vingt, INSERM, Institut de la Vision, GRC32, CIC1423, F-75012 Paris, France
[6]Sorbonne Université, CNRS, Laboratoire de Chimie de la Matière Condensée de Paris (LCMCP), Paris, F-75005, France
[7]Currently at Ecole Normale Supérieure, CNRS-ENS-SU UMR 8640, 24 rue Lhomond, Paris, F-75005, France
[8]Université Paris-Saclay, F-91406 Orsay, France
*Corresponding author: marie-claire.schanne-klein@polytechnique.edu

Received 2 June 2020; revised 21 July 2020; accepted 25 July 2020 (Doc. ID 399246); published 22 October 2020

Second-harmonic generation (SHG) microscopy is currently the preferred technique for visualizing collagen in intact tissues, but the usual implementations struggle to reveal collagen fibrils oriented out of the imaging plane. Recently, an advanced SHG modality, circular dichroism SHG (CD-SHG), has been proposed to specifically highlight out-of-plane fibrils. In this study, we present a theoretical analysis of CD-SHG signals that goes beyond the electric dipolar approximation to account for collagen chirality. We demonstrate that magnetic dipolar contributions are necessary to analyze CD-SHG images of human cornea sections and other collagen-rich samples. We show that the sign of CD-SHG signals does not reveal whether collagen fibrils point upwards or downwards as tentatively proposed previously. CD-SHG instead probes the polarity distribution of out-of-plane fibril assemblies at submicrometer scale, namely homogeneous polarity versus a mix of antiparallel fibrils. This makes CD-SHG a powerful tool for characterizing collagen organization in tissues, specifically the degree of disorder, which is affected during pathological remodeling. CD-SHG may thus serve to discriminate healthy and diseased collagen-rich tissues.

https://doi.org/10.1364/OPTICA.399246

1. INTRODUCTION

Collagen is the most abundant protein in mammals and a major component of connective tissues such as arteries, skin, bones and cornea. Fibrillar collagens are characterized by a hierarchical structure: triple helix molecules self-assemble into fibrils with 12 to > 500 nm diameter that further form various tridimensional (3D) structures at larger scales [1]. This 3D multiscale structure is a key distinctive feature of every tissue that governs its functional behavior, notably its mechanical properties [2]. For example, type I collagen thin fibrils self-assemble in a plywood-like structure in cornea, which is transparent and rigid, while thick fibrils form tangled threads in skin, which is opaque and resilient. A defective collagen 3D structure leads to tissue malfunctions, which is the case in many diseases featuring tissue remodeling [3]. *In situ* 3D imaging of collagen is therefore a major biomedical concern to decipher the relationship between structure and function in tissues and to implement sensitive and reliable diagnosis of diseases affecting collagen structure.

The gold standard technique for *in situ* 3D visualization of fibrillar collagen in intact tissues is second-harmonic generation (SHG) microscopy [4,5]. Advanced implementations of this technique include polarization-resolved (P-SHG) and interferometric (I-SHG) measurements [6–15]. Theoretical analyses of these modalities approximate the collagen molecule as a cylinder and neglect chiral components related to collagen helical structure in the SHG signal. They have shown that P-SHG and I-SHG provide invaluable information about the distribution of collagen fibrils in the imaging plane. However, these modalities do not provide any information about the out-of-plane organization of collagen fibrils, which is also of great interest to characterize collagen 3D structure. Out-of-plane direction can be estimated from 3D image stacks or

from P-SHG data (considering a fixed anisotropy parameter) in tissues with well-isolated fibrils or homogeneous structure [16–18] but cannot be reliably determined in most tissues composed of dense collagen networks with complex 3D orientations.

Circular dichroism SHG (CD-SHG) microscopy has been recently developed to address this issue. Similar to the first CD-SHG measurements developed in surface SHG in the 1990s [19,20], this new modality measures the normalized difference of the SHG signals excited with left-handed versus right-handed circular polarizations in chiral samples [21–27]. Recent reports have demonstrated that CD-SHG reveals collagen fibrils that are oriented out of the imaging plane, while in-plane fibrils show no or very low CD-SHG [22,23,26,27]. It has also been suggested that the sign of the CD-SHG correlates with the out-of-plane orientation (i.e., polarity) of the collagen fibrils, specifically that negative (resp. positive) CD-SHG reveals fibrils pointing downwards (resp. upwards) from the imaging plane [22,23,25,26]. However, no experimental demonstration of the variation of collagen CD-SHG with the out-of-plane orientation has been reported up to now. Indeed, these are challenging measurements because of the difficulty in having well-calibrated collagen samples with a perfectly known homogeneous structure and because CD-SHG is prone to experimental artifacts [27]. Moreover, no theoretical analysis of CD-SHG microscopy including magnetic dipolar effects has been reported up to now, although these magnetic effects have been shown to contribute strongly to surface CD-SHG signals in most chiral molecules [20,28,29], including collagen [30].

This study aims at deriving a theoretical analysis of CD-SHG signals that includes magnetic dipolar contributions and at elucidating what collagen structural information is provided by CD-SHG imaging. We first derive analytically and numerically the dependence of CD-SHG with the out-of-plane angle of collagen fibrils. We then compare these theoretical considerations to CD-SHG experiments on human corneas and other collagen-rich samples, which advantageously exhibit a well-defined structure. Our data show that the sign of CD-SHG does not indicate whether collagen fibrils point upwards or downwards, but instead probes the polarity distribution of out-of-plane fibril assemblies, which is an important parameter for biological tissues.

2. THEORETICAL BACKGROUND

Analytical calculation including magnetic dipolar contributions. CD-SHG is measured as the normalized difference between SHG signals $I_L^{2\omega}$ and $I_R^{2\omega}$ excited with a left circular (LCP) and a right circular (RCP) polarization [19,20]:

$$\text{CD-SHG} = \frac{I_L^{2\omega} - I_R^{2\omega}}{(I_L^{2\omega} + I_R^{2\omega})/2}. \quad (1)$$

In the electric dipolar approximation, the SHG response of collagen fibrils is described by a unique second-order susceptibility tensor, usually written as $\underline{\underline{\chi}}^{(2)}$ or χ^{eee} here, which exhibits a cylindrical symmetry C_∞ (Table 1). To take into account the chirality of collagen, we must go beyond this approximation and include the electric quadrupolar and magnetic dipolar contributions to the SHG signal [31]. As these two contributions cannot be distinguished experimentally, we consider only the magnetic ones χ^{eem} and χ^{mee} for the sake of simplicity, following the pioneering work by Persoons' group [32]. These magnetic tensors have the same cylindrical symmetry as the electric one χ^{eee} except that for χ^{eem}, it is not possible to interchange the last two indices (Table 1). Thus, we introduce a nonlinear magnetization at frequency 2ω $\vec{M}^{(2)}(2\omega)$ besides the nonlinear polarization $\vec{P}^{(2)}(2\omega)$ [32]:

Table 1. Nonzero Components of the SHG Susceptibility Tensors in the Cylindrical Symmetry C_∞[a]

	Electric Dipolar	Magnetic Dipolar	
Achiral	$\chi^{eee}_{xxx}, \chi^{eee}_{xyy} = \chi^{eee}_{xzz}, \chi^{eee}_{yxy} = \chi^{eee}_{yyx} = \chi^{eee}_{zxz} = \chi^{eee}_{zzx}$.	$\chi^{mee}_{yzx} = \chi^{mee}_{yxz} = \chi^{mee}_{zyx} = -\chi^{mee}_{zxy}$	$\chi^{eem}_{yzx} = -\chi^{eem}_{zyx}, \chi^{eem}_{yxz} = -\chi^{eem}_{zxy}, \chi^{eem}_{xyz} = -\chi^{eem}_{xzy}$.
Chiral	$\chi^{eee}_{yzx} = \chi^{eee}_{yxz} = -\chi^{eee}_{zyx} = -\chi^{eee}_{zxy}$	$\chi^{mee}_{xxx}, \chi^{mee}_{xyy} = \chi^{mee}_{xzz}, \chi^{mee}_{yxy} = \chi^{mee}_{yyx} = \chi^{mee}_{zxz} = \chi^{mee}_{zzx}$.	$\chi^{eem}_{xxx}, \chi^{eem}_{xyy} = \chi^{eem}_{xzz}, \chi^{eem}_{yxy} = \chi^{eem}_{zxz}, \chi^{eem}_{yyx} = \chi^{eem}_{zzx}$.

[a]Chiral (resp. achiral) components are nonzero only for chiral samples (resp. for any sample).

$$\vec{P}^{(2)}(2\omega) = \epsilon_0 \underline{\underline{\chi}}^{eee} \vec{E}(\omega)\vec{E}(\omega) + 2\epsilon_0 \underline{\underline{\chi}}^{eem} \vec{E}(\omega)\vec{B}(\omega),$$

$$\vec{M}^{(2)}(2\omega) = \epsilon_0 \underline{\underline{\chi}}^{mee} \vec{E}(\omega)\vec{E}(\omega). \quad (2)$$

They both act as sources for the second-harmonic field:

$$\vec{E}(2\omega) \propto (\hat{e}_Z \times \vec{P}^{(2)}(2\omega)) \times \hat{e}_Z - \hat{e}_Z \times \vec{M}^{(2)}(2\omega). \quad (3)$$

$\hat{e}_Z$ is the direction of propagation of the incident field $\vec{E}(\omega)$ at fundamental frequency. A circularly polarized incident field is used: $\vec{E}_{L/R}(\omega) = \frac{E_0}{\sqrt{2}}(\hat{e}_X \pm i\hat{e}_Y)$, where the subscript L (resp. R) stands for LCP (resp. RCP).

The CD-SHG signal can be derived analytically in the plane wave approximation, considering a homogeneous medium consisting of collagen fibrils aligned with each other, with no or little orientation dispersion in the focal volume. The associated frame is xyz, called the fibril frame, where x represents the mean orientation of the fibrils. It is linked to the laboratory frame XYZ by the φ and ψ Euler angles given in Fig. 1. Note that here the out-of-plane angle ψ varies from $-\pi/2$ to $\pi/2$, and the in-plane (azimuthal) angle φ from $-\pi$ to π.

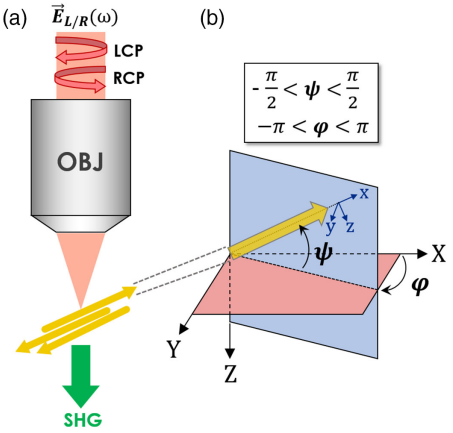

Fig. 1. Principle of CD-SHG measurement in collagen. (a) A LCP ($\vec{E}_L$) or RCP ($\vec{E}_R$) incident field is focused on collagen fibrils organized along one mean orientation. (b) φ and ψ angles connect the fibril frame xyz to the laboratory frame XYZ. The φ angle is the fibril mean angle in the imaging plane XY (light red color), ranging from $-\pi$ to π, while the ψ angle is the out-of-plane angle, ranging from $-\frac{\pi}{2}$ to $+\frac{\pi}{2}$.

The components of the susceptibility tensors are complex values and are referred to as chiral or achiral according to their symmetry (Table 1). Considering that all the tensor components of the same type have the same molecular origin, we assume that all the achiral (resp. chiral) components of the electric tensor χ^{eee} exhibit the same phase γ_A^e (resp. γ_C^e), as well as all the achiral (resp. chiral) components of the magnetic tensors χ^{mee} and χ^{eem} exhibit the same phase γ_A^m (resp. γ_C^m). This hypothesis advantageously results in tractable expressions that give an insight into the physics of CD-SHG signals. As the CD-SHG sign is given by its numerator since its denominator is always positive, we clarified here only the CD-SHG numerator (detailed calculation in Supplement 1.1):

$$\begin{aligned}\text{CD-SHG} = \frac{K(I^\omega)^2 \cos\psi}{I_{\mathrm{L}}^{2\omega} + I_{\mathrm{R}}^{2\omega}} \\ \times \Big[\left(\mathcal{A}_1^e\, \mathcal{C}_1^m + \mathcal{A}_2^e\, \mathcal{C}_2^m\right) \sin(\gamma_{\mathrm{C}}^m - \gamma_{\mathrm{A}}^e) \quad \text{(cross)} \\ + \mathcal{A}^m\, \mathcal{C}_3^e \sin(\gamma_{\mathrm{C}}^e - \gamma_{\mathrm{A}}^m) \quad \text{(cross)} \\ + \left(\mathcal{A}_1^e\, \mathcal{C}_1^e + \mathcal{A}_2^e\, \mathcal{C}_2^e\right) \sin(\gamma_{\mathrm{C}}^e - \gamma_{\mathrm{A}}^e) \quad \text{(electric)} \\ + \mathcal{A}^m\, \mathcal{C}_3^m \sin(\gamma_{\mathrm{C}}^m - \gamma_{\mathrm{A}}^m) \Big], \quad \text{(magnetic)},\end{aligned} \tag{4}$$

with

$$\begin{aligned}&\mathcal{A}_1^e = |\chi_{xxx}^{eee}| - |\chi_{xyy}^{eee}|, \quad \mathcal{A}_2^e = |\chi_{yxy}^{eee}|, \\ &\mathcal{A}^m = |\chi_{yzx}^{mee}| - \left(|\chi_{yzx}^{eem}| + |\chi_{yxz}^{eem}|\right), \\ &\mathcal{C}_1^e = 2\, \sin\psi\, \cos^2\psi |\chi_{yzx}^{eee}|, \quad \textbf{(odd)} \\ &\mathcal{C}_2^e = 4\, \sin\psi\, (1 + \sin^2\psi) |\chi_{yzx}^{eee}|, \quad \textbf{(odd)} \\ &\mathcal{C}_3^e = 8 \sin^2\psi |\chi_{yzx}^{eee}|, \\ &\mathcal{C}_1^m = 2\cos^2\psi \Big(\cos^2\psi (|\chi_{xxx}^{eem}| - |\chi_{xyy}^{eem}|) \\ &\qquad + \sin^2\psi (|\chi_{yxy}^{eem}| + |\chi_{yyx}^{eem}|) - |\chi_{yxy}^{mee}|\Big), \\ &\mathcal{C}_2^m = 4\sin^2\psi \cos^2\psi (|\chi_{xxx}^{eem}| - |\chi_{xyy}^{eem}|) \\ &\qquad + 4(1 + \sin^4\psi)(|\chi_{yxy}^{eem}| + |\chi_{yyx}^{eem}|) \\ &\qquad - 2\cos^2\psi (|\chi_{xxx}^{mee}| - |\chi_{xyy}^{mee}|) - 8\sin^2\psi |\chi_{yxy}^{mee}|, \\ &\mathcal{C}_3^m = 2\, \sin\psi\, [\, \cos^2\psi (2|\chi_{xxx}^{eem}| - 2|\chi_{xyy}^{eem}| - |\chi_{xxx}^{mee}| + |\chi_{xyy}^{mee}|) \\ &\qquad + 2(1 + \sin^2\psi)(|\chi_{yxy}^{eem}| + |\chi_{yyx}^{eem}| - |\chi_{yxy}^{mee}|)\,]. \quad \textbf{(odd)}\end{aligned} \tag{5}$$

Equation (4) shows that each contribution to the CD-SHG signal is a product between chiral and achiral tensor components, provided there is a phase shift between these components. Products of components from the same tensor types are called inner contributions: either *electric* ones (green × red) or *magnetic* ones (blue × pink). Products of components from different tensor types are called *cross* contributions: either between electric achiral components and magnetic chiral components (first term, green × pink) or between magnetic achiral components and electric chiral components (second term, blue × red).

Equation (5) shows that the sine of the out-of-plane angle $\sin\psi$ is a factor of all the electric and magnetic inner contributions, involving the chiral terms $\mathcal{C}_1^e$, $\mathcal{C}_2^e$, and $\mathcal{C}_3^m$, whereas $\sin\psi$ appears at an even power in the cross contributions, involving the chiral terms $\mathcal{C}_3^e$, $\mathcal{C}_1^m$, and $\mathcal{C}_2^m$. As a consequence, inner (resp. cross) contributions are odd (resp. even) functions of the out-of-plane angle ψ.

Numerical simulation of CD-SHG as a function of the collagen fibrils out-of-plane angle. We performed numerical simulations to get insight into the behavior of the different contributions to the CD-SHG. This behavior depends strongly on the modulus and phase of the different components of the three susceptibility tensors. Nevertheless, only the achiral electric components have been consistently measured by use of P-SHG imaging [6,7,9,33–35]. The main component is χ_{xxx}^{eee}, which is set to one and considered as the phase reference ($\gamma_A^e = 0$). The other achiral electric components are slightly smaller with the same phase; we set them to $\frac{1}{1.36}$ according to our measurements in rat-tail tendon and in cornea [9,35]. Theoretical analysis [31] and experimental measurements in other chiral molecules [36] show that all the other components are much smaller (typically $\frac{1}{10}$). Moreover, magnetic contributions exhibit a $\frac{\pi}{2}$ phase shift compared to the electric ones [31]. γ_C^e is therefore close to zero, while γ_A^m and γ_C^m are close to $\frac{\pi}{2}$. All our numerical simulations were then performed according to these orders of magnitude, unless otherwise specified (detailed values in Supplement 1 Tables S1 and S2).

Figure 2(a) shows numerical simulations of the inner and cross contributions to the CD-SHG as a function of the out-of-plane angle ψ. Regarding the cross contribution, the phase of the electric chiral component was set to zero and the one of the magnetic chiral and achiral components to $\frac{\pi}{2}$ as expected from theory. Regarding the inner contributions, a $\frac{\pi}{2}$ phase shift was imposed between the chiral and achiral components of the same tensors because the expected zero phase shift results in a vanishing CD-SHG. Figure 2(a) confirms that inner contributions are odd functions of the out-of-plane angle ψ, in agreement with previous derivations [22,23,37]. In contrast, the cross contribution, which is presumably the prevailing one as it complies with the expected $\frac{\pi}{2}$ phase shift between electric and magnetic contributions, is an even function of ψ.

The total CD-SHG obtained when merging all contributions was then investigated. Figure 2(b) shows numerical simulations of CD-SHG(ψ) when the phase of the chiral component of the electric tensor varies from $\frac{\pi}{32}$ (blue curve) to $\frac{\pi}{2}$ (green curve), with all other components remaining constant (Supplement 1 Table S1). The increase of γ_{C}^e transforms the profile CD-SHG(ψ) from an almost even function (blue curve) to an odd function that is shifted upwards (green curve). Indeed, the larger the chiral phase γ_C^e, the stronger the inner electric contribution, which scales as $\sin(\gamma_{\mathrm{C}}^e - \gamma_{\mathrm{A}}^e)$, which results in an odd behavior. On the contrary, a small electric chiral phase γ_{C}^e reduces the phase shift with the electric achiral components $\gamma_{\mathrm{C}}^e - \gamma_{\mathrm{A}}^e$ and increases the one with the magnetic achiral components $\gamma_{\mathrm{C}}^e - \gamma_{\mathrm{A}}^m$, which results in a prevailing cross contribution, i.e., an even behavior.

To sum up, depending on the γ_{C}^e phase value, the CD-SHG(ψ) curve is either of an *even* type or an *odd-shifted* type. Changing the phase and modulus of other tensor components can translate this curve upwards or downwards, or mirror the curve with respect to the horizontal axis. Typical examples are shown in Fig. 2(c)

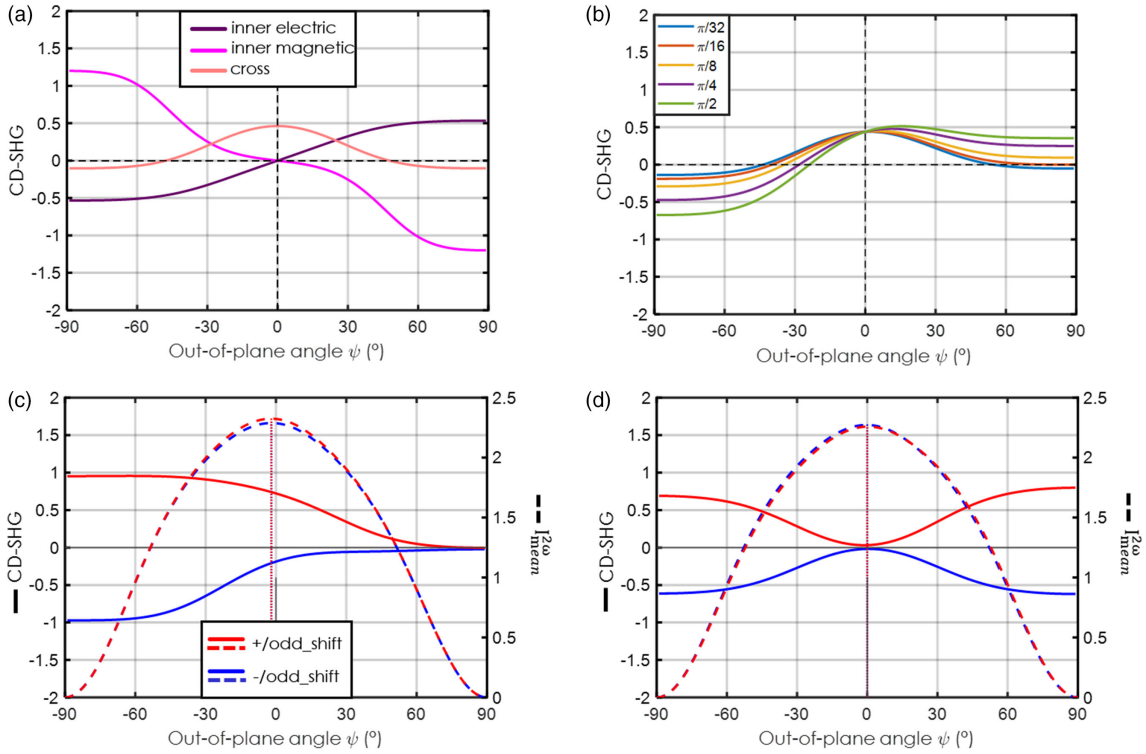

Fig. 2. Numerical simulations of the CD-SHG signal as a function of the out-of-plane angle ψ. (a) Each simulation corresponds to one isolated contribution to the CD-SHG signal, namely, inner *electric*, inner *magnetic*, or *cross* contributions [Eq. (4)], while the other ones are set to zero. (b) Each simulation corresponds to a particular phase γ_C^e of the chiral components of the electric tensor, varying from $\frac{\pi}{32}$ (blue curve) to $\frac{\pi}{2}$ (green curve), with all other components remaining constant. Tensor phases are $\gamma_A^e = 0$, $\gamma_A^m = \frac{\pi}{2}$ and $\gamma_C^m = \frac{2\pi}{5}$. (c) Typical odd-shifted cases corresponding to prevailing inner contributions, with either fully positive or negative CD-SHG values. (d) Typical even cases corresponding to predominant cross contributions, with either fully positive or negative CD-SHG values. In (c) and (d), CD-SHG is plotted in solid lines and SHG intensity in dotted lines. Tensor components used for each simulation are given in Tables S1 and S2.

[resp. Fig. 2(d)], where the odd-shifted (resp. even) curve is shifted downwards to negative CD-SHG values (blue solid line) and roughly mirrored with respect to the horizontal axis (red solid line) (Supplement 1 Table S2). Figures 2(c) and 2(d) also show in dotted lines numerical simulations of the mean SHG intensity $I^{2\omega}_{\text{mean}} = \frac{1}{2}(I^{2\omega}_{\text{L}} + I^{2\omega}_{\text{R}})$, which is consistently maximal when the out-of-plane angle ψ is small, namely for in-plane structures. At this intensity maximum, the CD-SHG signal may be also quite high, as in the odd-shifted case, or may vanish as in the even case.

3. CD-SHG EXPERIMENTS IN COLLAGENEOUS TISSUES

Experimental setup. SHG imaging was performed on two different setups. The first setup was a custom-built laser scanning upright multiphoton microscope with femtosecond titanium:sapphire laser excitation (MaiTai, SpectraPhysics) at 860 nm as previously described [27,38]. Laser power was less than 10 mW at the sample, with 10 to 20 µs/pixel dwell time and 0.1 to 0.2 µm pixel size. A high numerical aperture objective with water immersion (25×, NA 1.05, Plan-Apochromat, Olympus) was used to achieve approximately 0.4 µm lateral × 1.2 µm axial resolutions near the sample surface. SHG signals were detected in the forward direction (U-AAAC aplanetic condenser 1.4 NA, Olympus) using a photon-counting photomultiplier tube (P25PC, SensTech) and suitable spectral filters (FF01-720/SP, FF01-680/SP and FF01-427/10, Semrock). The second setup used for fascia imaging is very similar as described in [39].

Two SHG images were recorded sequentially, using incident RCP and LCP excitations. Then the CD-SHG (normalized difference of the two images) and the average SHG intensity (average of the two images) were computed pixel-wise. A thorough protocol, described in [27], was used to perform artifact-free CD-SHG measurements. Specifically, we optimized: (i) the stability of the sample holder in order to avoid artifacts due to a spatial drift of the sample between the first acquisition with LCP excitation and the second one with RCP excitation; (ii) the circularity of the incident polarizations (ellipticity larger than 0.98, see Supplement 1.3) in order to avoid artifacts due to linear dichroism. Moreover, we accumulated several acquisitions to increase the accuracy of the CD-SHG measurements. The precision was 0.1 for eight accumulated images and SHG intensity of 20 photons. To verify the validity of our measurements, we checked that the CD-SHG signal did not depend on the in-plane angle φ of the sample as expected for circularly polarized excitation (Supplement 1 Fig. S1). CD-SHG images are presented using a blue-white-red color chart for values in the $[-1; 1]$ interval and saturated blue/red colors outside this interval ($[-2, -1$ [and] $1,2]$ as CD-SHG signal belongs to the interval $[-2, 2]$). Black pixels correspond to undefined CD-SHG, due to a poor signal-to-noise ratio.

Experimental results. We explored the dependence of CD-SHG on the out-of-plane orientation by imaging the very same region of collagen thin samples in the *up* and *down* configurations,

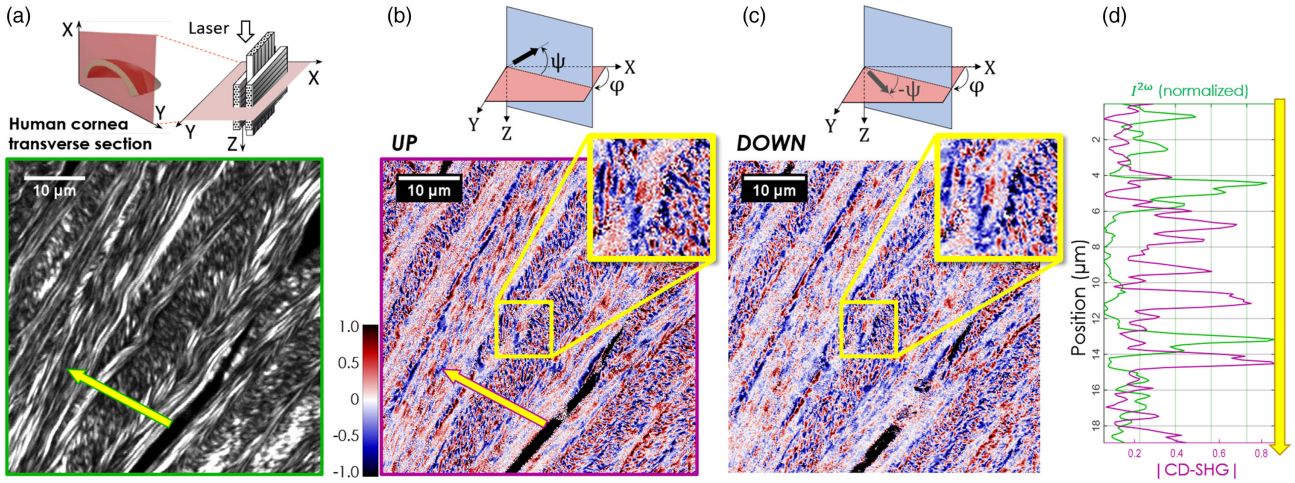

Fig. 3. *Up/down* CD-SHG imaging of a human cornea transverse section. (a) Scheme of the sample and mean SHG intensity image in the *up* configuration. (b), (c) CD-SHG images of the same region of interest in the (b) *up* and (c) *down* configurations and corresponding schemes. The sign of the CD-SHG is the same in the two configurations for 80% of the pixels. (d) Profile plots of the SHG intensity (green) and the absolute value of CD-SHG (magenta), along the yellow arrow in (a) and (b).

i.e., before and after rotation of the samples by π with respect to the X axis of the laboratory frame. The *down* image is then digitally flipped with respect to the same axis to facilitate the comparison between the two images (top schemes in Fig. 3): the out-of-plane angle is opposite $\psi_{\text{down}} = -\psi_{\text{up}}$, while the in-plane angle is unchanged $\varphi_{\text{down}} = \varphi_{\text{up}}$.

These *up/down* experiments were conducted on various thin collagen-rich samples: six transverse sections of human corneas (18 CD-SHG images in total), *in vitro* isolated collagen fibrils, and collagen fibrillar membranes on a first setup and a section of murine fascia on a second setup (Supplement 1.2). All samples were a few µm thin to avoid any distortion of polarization upon propagation in depth and to enable *up/down* experiments. The human cornea is composed of thin collagen fibrils aligned within 1–3 µm thick lamellae superimposed along the depth of the cornea, parallel to its surface [40] (Supplement 1 Fig. S2). These lamellae are oriented mainly along two perpendicular directions, so that cornea transverse sections exhibit regions with in-plane fibrils and others with out-of-plane fibrils [inset in Fig. 3(a)]. Murine fascia sections and collagen membranes also display a wide distribution of out-of-plane fibrils, while *in vitro* collagen fibrils are mainly in-plane structures.

Typical results obtained on a transverse section of a human cornea are displayed in Figs. 3 and 4. The other samples exhibit a similar behavior, as shown in Supplement 1 Figs. S3 to S5. First, we observe that the CD-SHG signal takes both positive and negative values in a same sample, while the CD-SHG absolute value depends on the type of sample. In *in vitro* isolated collagen fibrils with vanishing out-of-plane angles, the mean CD-SHG absolute value is low, around 0.1. In the other samples with out-of-plane fibrils, the mean CD-SHG absolute value is higher: about 0.3 in cornea, 0.2 in murine fascia, and 0.15 to 0.3 in collagen membranes. More precisely, out-of-plane fibrils can be identified by a smaller SHG intensity than the one exhibited by in-plane fibrils because the SHG intensity has been shown to scale as the squared cosine of the out-of-plane angle [16–18]. We therefore plotted profiles of the CD-SHG absolute value and the SHG intensity [Fig. 3(d)] and observed as expected an anti-correlation: a low CD-SHG absolute value corresponds to high SHG intensity, which is indicative of in-plane structures, while a high CD-SHG absolute value corresponds to low SHG intensity, which is indicative of out-of-plane structures. Quantitative processing of all the cornea images shows that the normalized SHG intensity is 1.5 higher in pixels exhibiting a low CD-SHG absolute value (<0.2) than in those exhibiting a large one (≥ 0.2) and that this difference is significant (Supplement 1.4 and Fig. S6). This confirms previous reports showing that CD-SHG efficiently reveals collagen fibrils directed out of the imaging plane [22,23,26,27].

Second, we observe that the CD-SHG signal is the same in the *up* and *down* configurations, as illustrated in Figs. 3(b), 3(c), 4(a), and 4(b). Especially, we do not observe any sign reversal of the CD-SHG signal between these two configurations: a positive (resp. negative) signal for an angle ψ remains a positive (resp. negative) signal for the opposite angle $-\psi$, as illustrated in the profiles displayed in Fig. 4(c). Quantitation of the CD-SHG images of the six corneas under study show that the sign of the CD-SHG is the same in 75±6% of the pixels for the *up* and *down* configurations (Supplement 1.4). This unexpected result is also obtained in our

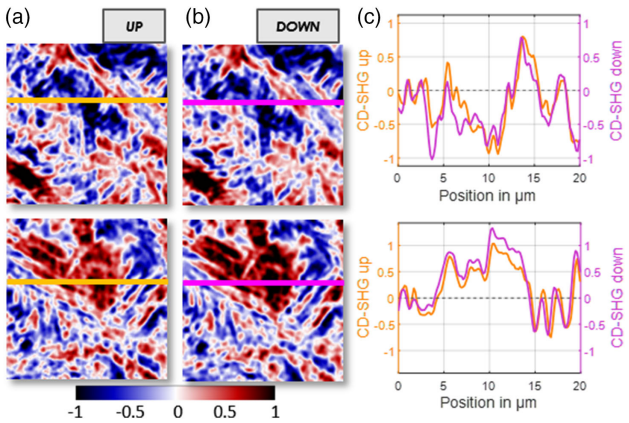

Fig. 4. *Up/down* CD-SHG profiles in a transverse section of human cornea. (a), (b) Zoomed-in CD-SHG images of the same region of interest in the (a) *up* and (b) *down* configurations (10× 10 µm²). (c) Profiles of the CD-SHG signals along the lines in (a) and (b). The sign of the CD-SHG is the same in 90% of the pixels.

other collagen samples, regardless of the experimental setup used for the measurements (Supplement 1 Figs. S3 to S5). Yet, this is not observed in a $LiIO_3$ crystal, which exhibits the same C_∞ symmetry as collagen fibrils and was therefore used as a control sample. CD-SHG measurements on the two opposite sides of the crystal, which corresponds to opposite orientations of the optical axis, showed opposite CD-SHG signals (Supplement 1 Fig. S7).

We also performed experiments on tilted samples that provide the absolute value of the slope of the function CD-SHG(ψ) (Supplement 1.5). Our results on human corneas show that the slope of CD-SHG(ψ) is low for small CD-SHG signals and increases for larger CD-SHG signals (Supplement 1 Fig. S8).

4. DISCUSSION

Chirality is present in collagen at all structural scales: peptide units are L-amino acids, tropocollagen molecules are composed of three left-handed α chains wound together as a right-handed triple helix, and fibrils show a left-handed helical twist [41–43]. Collagen thus exhibits optical activity, notably circular dichroism (CD), which is theoretically accounted for by the introduction of magnetic dipolar and electric quadrupolar terms [31]. CD-SHG is the nonlinear analog of conventional (linear) CD. It was first demonstrated in the framework of surface SHG experiments on chiral molecular films, including collagen [19,30,32]. The underlying physical mechanisms have been investigated by introducing nonlinearities in the two classical models of conventional optical activity. The one-electron model [44] describes chiral molecules exhibiting a chiral center or an helical structure, i.e. an optical transition with both an electric and a magnetic dipole [44]. The coupled-oscillator model [45] describes molecules with a chiral arrangement of achiral chromophores, i.e. the coupling of two noncoplanar electric dipoles. Generalization of the one-electron model to SHG shows that CD-SHG originates from magnetic dipolar and electric quadrupolar contributions, as in linear optics [28,29]. This was first observed by Persoons' group [32], who introduced the χ^{eem} and χ^{mee} susceptibility tensors. In contrast, the introduction of nonlinearities in the coupled-oscillator model results in a nonvanishing chiral component of the usual electric dipolar susceptibility χ^{eee}_{yzx} [28,46]. It means that SHG optical activity can also exist in a purely electric dipolar approach. Indeed, SHG susceptibility is a third-rank tensor and therefore directly probes chirality in 3D, as first proposed by Hicks' group [47].

In this paper, we have extended this approach to the theoretical analysis of CD-SHG microscopy. Equations (4) and (5) show what conditions are required for nonzero CD-SHG: chiral susceptibility components must be nonzero and phase shifted compared to the achiral ones. This key feature of CD-SHG, also present in surface SHG experiments, is obtained easily when the chiral components come from the magnetic susceptibility tensors χ^{eem} and χ^{mee}. Indeed, magnetic dipolar components exhibit a $\pi/2$ phase shift compared to electric dipolar ones, which are the main achiral components. This makes CD-SHG sensitive mainly to one-electron chirality because chiral components in the one-electron model are found mostly in the magnetic tensors χ^{eem} and χ^{mee}. In contrast, in the coupled-oscillator model, the main chiral susceptibility component χ^{eee}_{yzx} involves only electric dipolar transitions. It can be phase shifted compared to achiral components only if these two types of components are affected by different resonances, which cannot be ruled out in collagen, given the complexity of its nonlinear response [48].

These two types of contributions to the CD-SHG signal were therefore explored by numerical simulations. Electric chiral contributions correspond to a γ^e_C phase close to $\pi/2$. It results in an odd function of the out-of-plane angle ψ because of the sin ψ variation of $\mathcal{C}^e_1$ and $\mathcal{C}^e_2$ [(Eq. (5)], which means that the CD-SHG sign reveals the out-of-plane orientation of collagen fibrils [purple curve in Fig. 2(a)]. This curve may be slightly altered and shifted when small magnetic contributions are also present [Fig. 2(c) and green curve in Fig. 2(b)]. However, this odd-shifted curve still presents different CD-SHG signals for opposite orientations. In contrast, prevailing magnetic contributions correspond to prevailing cross terms between electric achiral and magnetic chiral components in Eq. (4). Given that $\mathcal{C}^m_1$ and $\mathcal{C}^m_2$ involve even powers of sin ψ [(Eq. (5)], this contribution is an even function of the out-of-plane angle [orange curve in Fig. 2(a)]. It is therefore not sensitive to the fibrils' polarity, even when small electric contributions alter slightly the symmetry of the CD-SHG(ψ) function [Fig. 2(d) and blue curve in Fig. 2(b)].

Up/down CD-SHG images recorded on several types of collagen samples using two different setups unambiguously demonstrate that the CD-SHG sign does not reveal the collagen out-of-plane polarity. This result cannot be accounted for by previous phenomenological approaches in the electric dipolar approximation [22,24,26]. It therefore confirms the relevance of our theoretical analysis based on χ^{eem} and χ^{mee} susceptibility tensors. Most importantly, it indicates that the collagen CD-SHG is dominated by these magnetic contributions and originates largely from one-electron chirality. Other materials characterized by excitonic coupling chirality may behave differently [29,47]. It is presumably the case for $LiIO_3$ crystal, whose CD-SHG appears to be dominated by inner electric contributions and changes sign in the *up* and *down* configurations, as in Fig. 2(a).

Figure 3(d) and Supplement 1 Fig. S3, however, confirm that CD-SHG highlights out-of-plane fibrils and vanishes for in-plane fibrils. This is consistent with the numerical simulations depicted in Fig. 2(d), which show even curves vanishing at $\psi = 0$. Experiments on tilted samples also agree with these numerical simulations, as smaller slopes are observed around $\psi = 0$ (Supplement 1 Fig. S8). The fully positive or fully negative even curve depicted in Fig. 2(d) therefore appears to estimate at best the dependence of CD-SHG with the out-of-plane collagen angle.

Strikingly, all our samples show positive and negative CD-SHG signals in different regions. It means that our data can be reproduced by either the fully positive curve (red) or the fully negative one (blue) depicted in Fig. 2(d), depending on every pixel. These positive and negative CD-SHG curves are obtained for different moduli of the chiral components used in the numerical simulations, while the achiral ones are fixed (Supplement 1 Table S2). It indicates that the relative values of these chiral components compared to the achiral ones may vary within a sample. This is not surprising because chiral and achiral susceptibility components do not behave the same way as a function of fibril orientation. Achiral components cancel out for assemblies of fibrils with opposite orientations in the focal volume, while chiral components add up [Supplement 1 Figs. S9(a) and S9(b)]. This is equally valid for electric and magnetic susceptibilities because it derives from intrinsic symmetry properties of third-rank tensors. Accordingly, the values of the chiral components relative to the achiral ones vary

in the parallel and anti-parallel geometries. These variations are, however, complex because they depend on the directions of the dipole transitions involved in the SHG response at the molecular scale, so that it is not possible yet to link the sign of the CD-SHG to a specific geometry. Our results still show unambiguously that CD-SHG probes the polarity distribution of fibril assemblies, which is the degree of polar order at sub-μm scale, for instance fibrils all pointing in the same direction versus a mix of fibrils pointing upwards and downwards [Supplement 1 Figs. S9(c) an S9(d)]. It is complementary to P-SHG, which is not sensitive to polarity and probes only the relative value of achiral components. This new structural probe is presumably sensitive to scales down to a few 10s of nm because thin fibrils may reverse orientation at these scale in various tissues, including cornea, as shown by I-SHG for in-plane fibrils [14].

5. CONCLUSION

CD-SHG is a unique SHG modality for two reasons. First, it highlights fibrils that are directed out of the imaging plane and therefore provides an efficient way to characterize collagen 3D distribution. This is crucial in dense and heterogeneous collagen networks as well as in thin histological sections, where 3D measurements are either ambiguous or impossible. Second, it probes the polarity distribution of out-of-plane fibrils at sub-μm scale. Importantly, it cannot discriminate whether the fibrils point mainly upwards or downwards in the imaging plane. From this point of view, it is in contrast to I-SHG, which reveals the fibrils' relative orientation in the imaging plane [14]. Sensitivity to the polarity distribution of out-of-plane fibril assemblies is necessary to reveal regions with random orientations or interfaces between domains with opposite orientations. This is crucial in many tissues, as anticipated in the pioneer article on collagen SHG by Freund *et al.* in 1982 [49], and particularly relevant in pathological remodeling, which is characterized by disordered collagen. Thus, in addition to deepening the microstructure/function relationship in complex tissues, CD-SHG opens up new opportunities for diagnosis of pathological tissues.

Funding. Ecole Doctorale Interfaces (ED573); Agence Nationale de la Recherche (ANR-10-INBS-04, ANR-11-EQPX-0029).

Acknowledgment. The authors thank Christian Pfeffer from the Harvard School of Dental Medicine for providing the murine fascia, Etablissement Français du Sang (EFS, Paris) and Banque Française des Yeux (BFY, Paris) for providing human corneas, Karin Schlattmann and Michèle Savoldelli for preparing the human cornea sections, Xavier Solinas and Jean-Marc Sintès for technical support in the SHG setup, and Willy Supatto, Emmanuel Beaurepaire, Pascale Changenet, and François Hache for fruitful discussions.

Disclosures. The authors declare no conflicts of interest.

See Supplement 1 for supporting content.

REFERENCES

1. D. Hulmes, "Building collagen molecules, fibrils, and suprafibrillar structures," J. Struct. Biol. **137**, 2–10 (2002).
2. K. L. Goh, A. Listrat, and D. Bechet, "Hierarchical mechanics of connective tissues: integrating insights from nano to macroscopic studies," J. Biomed. Nanotechnol. **10**, 2464–2507 (2014).
3. P. Fratzl and R. Weinkamer, "Nature's hierarchical materials," Prog. Mater. Sci. **52**, 1263–1334 (2007).
4. X. Y. Chen, O. Nadiarynkh, S. Plotnikov, and P. J. Campagnola, "Second harmonic generation microscopy for quantitative analysis of collagen fibrillar structure," Nat. Protocols **7**, 654–669 (2012).
5. S. Bancelin, C. Aimé, I. Gusachenko, L. Kowalczuk, G. Latour, T. Coradin, and M.-C. Schanne-Klein, "Determination of collagen fibril size via absolute measurements of second-harmonic generation signals," Nat. Commun. **5**, 4920 (2014).
6. P. Stoller, K. Reiser, P. Celliers, and A. Rubenchik, "Polarization-modulated second harmonic generation in collagen," Biophys. J. **82**, 3330–3342 (2002).
7. F. Tiaho, G. Recher, and D. Rouède, "Estimation of helical angle of myosin and collagen by second harmonic generation imaging microscopy," Opt. Express **15**, 12286–12295 (2007).
8. A. E. Tuer, M. K. Akens, S. Krouglov, D. Sandkuijl, B. C. Wilson, C. M. Whyne, and V. Barzda, "Hierarchical model of fibrillar collagen organization for interpreting the second-order susceptibility tensors in biological tissue," Biophys. J. **103**, 2093–2105 (2012).
9. I. Gusachenko, V. Tran, Y. Goulam Houssen, J.-M. Allain, and M.-C. Schanne-Klein, "Polarization-resolved second-harmonic generation in tendon upon mechanical stretching," Biophys. J. **102**, 2220–2229 (2012).
10. J. Duboisset, D. Ait-Belkacem, M. Roche, H. Rigneault, and S. Brasselet, "Generic model of the molecular orientational distribution probed by polarization-resolved second-harmonic generation," Phys. Rev. A **85**, 043829 (2012).
11. C. P. Brown, M. A. Houle, K. Popov, M. Nicklaus, C. A. Couture, M. Laliberté, T. Brabec, A. Ruediger, A. J. Carr, A. J. Price, H. S. Gill, L. Ramunno, and F. Légaré, "Imaging and modeling collagen architecture from the nano to micro scale," Biomed. Opt. Express **5**, 233–243 (2014).
12. A. Golaraei, L. Kontenis, R. Cisek, D. Tokarz, S. J. Done, B. C. Wilson, and V. Barzda, "Changes of collagen ultrastructure in breast cancer tissue determined by second-harmonic generation double Stokes-Mueller polarimetric microscopy," Biomed. Opt. Express **7**, 4054–4068 (2016).
13. A. Benoit, G. Latour, M.-C. Schanne-Klein, and J.-M. Allain, "Simultaneous microstructural and mechanical characterization of human corneas at increasing pressure," J. Mech. Behav. Biomed. Mater. **60**, 93–105 (2016).
14. M. Rivard, K. Popov, C.-A. Couture, M. Laliberté, A. Bertrand-Grenier, F. Martin, H. Pépin, C. P. Pfeffer, C. Brown, L. Ramunno, and F. Légaré, "Imaging the noncentrosymmetric structural organization of tendon with interferometric second harmonic generation microscopy," J. Biophoton. **7**, 638–646 (2014).
15. C.-A. Couture, S. Bancelin, J. Van der Kolk, K. Popov, M. Rivard, K. Légaré, G. Martel, H. Richard, C. Brown, S. Laverty, L. Ramunno, and F. Légaré, "The impact of collagen fibril polarity on second harmonic generation microscopy," Biophys. J. **109**, 2501–2510 (2015).
16. S. Psilodimitrakopoulos, I. Amat-Roldan, P. Loza-Alvarez, and D. Artigas, "Effect of molecular organization on the image histograms of polarization SHG microscopy," Biomed. Opt. Express **3**, 2681–2693 (2012).
17. C. Teulon, A. Tidu, F. Portier, G. Mosser, and M.-C. Schanne-Klein, "Probing the 3D structure of cornea-like collagen liquid crystals with polarization-resolved SHG microscopy," Opt. Express **24**, 16084–16098 (2016).
18. E. I. Romijn, A. Finnoy, and M. B. Lilledahl, "Analyzing the feasibility of discriminating between collagen types I and II using polarization-resolved second harmonic generation," J. Biophoton. **12**, e201800090 (2019).
19. T. P. Petralli-Mallow, T. M. Wong, J. D. Byers, H. I. Yee, and J. M. Hicks, "Circular dichroism spectroscopy at interfaces: a surface second harmonic generation study," J. Phys. Chem. **97**, 1383–1388 (1993).
20. T. Verbiest, M. Kauranen, A. Persoons, M. Ikonen, J. Kurkela, and H. Lemmetyinen, "Nonlinear optical activity and biomolecular chirality," J. Am. Chem. Soc. **116**, 9203–9205 (1994).

21. X. Chen, C. Raggio, and P. J. Campagnola, "Second-harmonic generation circular dichroism studies of osteogenesis imperfecta," Opt. Lett. **37**, 3837–3839 (2012).
22. H. Lee, M. J. Huttunen, K.-J. Hsu, M. Partanen, G.-Y. Zhuo, M. Kauranen, and S.-W. Chu, "Chiral imaging of collagen by second-harmonic generation circular dichroism," Biomed. Opt. Express **4**, 909–916 (2013).
23. G.-Y. Zhuo, M.-Y. Chen, C.-Y. Yeh, C.-L. Guo, and F.-J. Kao, "Fast determination of three-dimensional fibril orientation of type-I collagen via macroscopic chirality," Appl. Phys. Lett. **110**, 093902 (2017).
24. K. R. Campbell and P. J. Campagnola, "Wavelength-dependent second harmonic generation circular dichroism for differentiation of Col I and Col III isoforms in stromal models of ovarian cancer based on intrinsic chirality differences," J. Phys. Chem. B **121**, 1749–1757 (2017).
25. M.-Y. Chen, M. Huttunen, C.-W. Kan, G. Deka, Y.-Y. Lin, C.-W. Ye, M.-J. Wu, H.-L. Liu, and S.-W. Chu, "Resonant nonlinear microscopy reveals changes in molecular level chirality," Opt. Commun. **422**, 56–63 (2018).
26. A. Golaraei, L. Kontenis, K. Mirsanaye, S. Krouglov, M. K. Akens, B. C. Wilson, and V. Barzda, "Complex susceptibilities and chiroptical effects of collagen measured with polarimetric second-harmonic generation microscopy," Sci. Rep. **9**, 12488 (2019).
27. M. Schmeltz, C. Teulon, G. Latour, D. Ghoubay, V. Borderie, C. Aimé, and M.-C. Schanne-Klein, "Implementation of artifact-free circular dichroism SHG imaging of collagen," Opt. Express **27**, 22685–22699 (2019).
28. F. Hache, H. Mesnil, and M. C. Schanne-Klein, "Application of classical models of chirality to surface second harmonic generation," J. Chem. Phys. **115**, 6707–6715 (2001).
29. M.-C. Schanne-Klein, F. Hache, T. Brotin, C. Andraud, and A. Collet, "Magnetic chiroptical effects in surface second harmonic reflection," Chem. Phys. Lett. **338**, 159–166 (2001).
30. A. M. Pena, T. Boulesteix, T. Dartigalongue, and M. C. Schanne-Klein, "Chiroptical effects in the second harmonic signal of collagens I and IV," J. Am. Chem. Soc. **127**, 10314–10322 (2005).
31. G. Wagnière, *Linear and Nonlinear Optical Properties of Molecules* (Helvetica Chimica Acta, 1993).
32. M. Kauranen, S. Verbiest, J. J. Maki, and A. Persoons, "Second-harmonic generation from chiral surfaces," J. Chem. Phys. **101**, 8193–8199 (1994).
33. O. Nadiarnykh and P. J. Campagnola, "Retention of polarization signatures in SHG microscopy of scattering tissues through optical clearing," Opt. Express **17**, 5794–5806 (2009).
34. P.-J. Su, W.-L. Chen, Y.-F. Chen, and C.-Y. Dong, "Determination of collagen nanostructure from second-order susceptibility tensor analysis," Biophys. J. **100**, 2053–2062 (2011).
35. G. Latour, I. Gusachenko, L. Kowalczuk, I. Lamarre, and M.-C. Schanne-Klein, "In vivo structural imaging of the cornea by polarization-resolved second harmonic microscopy," Biomed. Opt. Express **3**, 1–15 (2012).
36. M. Kauranen, J. J. Maki, T. Verbiest, S. Van Elshocht, and A. Persoons, "Quantitative determination of electric and magnetic second-order susceptibility tensors of chiral surfaces," Phys. Rev. B **55**, R1985–R1988 (1997).
37. A. Golaraei, K. Mirsanaye, Y. Ro, S. Krouglov, M. K. Akens, B. C. Wilson, and V. Barzda, "Collagen chirality and three-dimensional orientation studied with polarimetric second-harmonic generation microscopy," J. Biophoton. **12**, e201800241 (2019).
38. C. Teulon, I. Gusachenko, G. Latour, and M.-C. Schanne-Klein, "Theoretical, numerical and experimental study of geometrical parameters that affect anisotropy measurements in polarization-resolved SHG microscopy," Opt. Express **23**, 9313–9328 (2015).
39. M. Pinsard, S. Laverty, H. Richard, J. Dubuc, M.-C. Schanne-Klein, and F. Légaré, "Maturation of the meniscal collagen structure revealed by polarization-resolved and directional second harmonic generation microscopy," Sci. Rep. **9**, 18448 (2019).
40. J. Krachmer, M. Mannis, and E. Holland, *Cornea*, 3rd ed. (Mosby Elsevier, 2011).
41. K. Beck and B. Brodsky, "Supercoiled protein motifs: the collagen triple-helix and the alpha-helical coiled coil," J. Struct. Biol. **122**, 17–29 (1998).
42. D. J. Prockop and A. Fertala, "The collagen fibril: the almost crystalline structure," J. Struct. Biol. **122**, 111–118 (1998).
43. M. Raspanti, M. Reguzzoni, M. Protasoni, and D. Martini, "Evidence of a discrete axial structure in unimodal collagen fibrils," Biomacromolecules **12**, 4344–4347 (2011).
44. W. Kauzmann, *Quantum Chemistry* (Academic, 1957).
45. W. Kuhn, "Quantitative verhältnisse und beziehungen bei der natürlichen optischen aktivität," Z. Phys. Chem. Abt. B **4**, 14 (1929).
46. M.-C. Schanne-Klein, T. Boulesteix, F. Hache, M. Alexandre, G. Lemercier, and C. Andraud, "Strong chiroptical effects in surface second harmonic generation obtained for molecules exhibiting excitonic coupling chirality," Chem. Phys. Lett. **362**, 103–108 (2002).
47. J. D. Byers, H. I. Yee, T. Petralli-Mallow, and J. M. Hicks, "2nd-harmonic generation circular-dichroism spectroscopy from chiral monolayers," Phys. Rev. B **49**, 14643–14647 (1994).
48. A. E. Tuer, S. Krouglov, N. Prent, R. Cisek, D. Sandkuijl, K. Yasufuku, B. C. Wilson, and V. Barzda, "Nonlinear optical properties of type I collagen fibers studied by polarization dependent second harmonic generation microscopy," J. Phys. Chem. B **115**, 12759–12769 (2011).
49. S. Roth and I. Freund, "Optical second-harmonic scattering in rat-tail tendon," Biopolymers **20**, 1271–1290 (1981).